International Journal of Heat and Mass Transfer 108 (2017) pp. 784-800
DOI:10.1016/j.ijheatmasstransfer.2016.12.069

Upward gas–liquid two-phase flow after a U-bend in a large-diameter serpentine pipe

Aliyu M. Aliyu[1], Almabrok A. Almabrok[2], Yahaya D. Baba[3], Liyun Lao[3], Hoi Yeung[3], Kyung Chun Kim[1*]

[1]School of Mechanical Engineering, Pusan National University, 609-735, Busan, Republic of Korea
[2]Department of Petroleum Engineering, Faculty of Engineering, Sirte University, Sirte, Libya
[3]Oil and Gas Engineering Centre, Cranfield University, Bedfordshire MK43 0AL, United Kingdom

Abstract

We present an experimental study on the flow behaviour of gas and liquid in the upward section of a vertical pipe system with an internal diameter of 101.6 mm and a serpentine geometry. The experimental matrix consists of superficial gas and liquid velocities in ranges of 0.15 to 30 m/s and from 0.07 to 1.5 m/s, respectively, which cover bubbly to annular flow. The effects on the flow behaviours downstream of the 180° return bend are significantly reduced when the flow reaches an axial distance of 47 pipe diameters from the U-bend. Therefore, reasonably developed flow is attained at this development length downstream of the bend. Other published measurements for large-diameter film thickness show similar trends with respect to the superficial gas velocity. However, the trends differ from those of small-diameter pipes, with which the film thickness decreases much faster with increasing gas flow. As a result, only a few of the published correlations for small pipe data agreed with the experimental data for large pipe film thickness. We therefore modified one of the best-performing correlations, which produced a better fit. Qualitative and statistical analyses show that the new correlation provides improved predictions for two-phase flow film thickness in large-diameter pipes.

Keywords: conductance film probes, large diameter pipes, multiphase flow, return bends, wire mesh sensor.

1 Introduction

Gas–liquid two-phase flows are frequently encountered in the chemical, process, and petroleum industries, where they are found in pipes with serpentine configurations in many cases. These configurations are applied in refrigeration, chemical plants, petroleum refineries, and power stations. Normally, the flow may either be single phase (liquid or gas) or two-phase, where both gas and liquid flow together, depending on the properties and operating conditions. Gas–liquid two-phase flows impose difficult problems on the design and operation of heat exchange facilities. For example, uneven liquid films along the pipe walls could create local dry spots and lead to boiling crises, which can cause catastrophic failures. This can lead to unplanned plant shutdowns, increase maintenance expenditure, and adversely impact on plant profitability.

*Corresponding author
E-mail address: kckim@pusan.ac.kr (K.C. Kim)

Preventing such occurrences requires thorough understanding of the multiphase phenomena, behaviour around return bends, and downstream impacts. When fluids flow through a bend, the centrifugal force generated causes flow maldistribution along the pipe cross-section. This effect is stronger for gas–liquid flows due to the substantial density difference between the phases. The influence of the centrifugal force on the phase distribution is transferred to the straight sections of the conduit after the bend. Several studies have examined the effects of return bends on the two-phase flow behaviour in the bends and pipe straights. However, these studies are mainly on pipes with 50-mm internal diameter or less. For example, Anderson and Hills [1] studied liquid film behaviours in return bends of 25.4-mm diameter for different orientations. Oshinowo and Charles [2] also investigated the effect of a return bend on the void fraction in a 25.4-mm vertical pipe with a serpentine geometry. They applied a force balance between the centrifugal and gravitational forces acting on the phases in the bend to explain the observed phase maldistributions in air/water and air/glycerol flows.

Abdulkadir et al. [3] studied the effect of a U-bend on the average film fraction within a bend and after in a 127-mm-diameter pipe system. They used a modified form of Oshinowo and Charles' [2] Froude number method to determine the phase occupying the outside of the bend with respect to the sign of the Froude number. They reported downstream effects for only a downward orientation due to the configuration of the flow facility, but the study provides no information on upward flow effects. Similarly, Almabrok et al. [4] focused on the effect of the bend on the downstream downward-flowing pipe section. While Abdulkadir et al. [3] used only conductance rings as instrumentation, Almabrok et al. [4] used a capacitance wire mesh sensor (WMS) and flush-mounted conductance probes.

There is a strong need to extend the knowledge of multiphase flow behaviour to systems with pipe diameters greater than 100 mm [5]–[13]. Conditions that produce bullet-shaped Taylor bubbles in pipes of less than 100-mm diameter do not do so in large-diameter pipes. This phenomenon is well documented [7], [12]–[16]. Without this consideration, incorrect flow regime predictions might lead to inappropriate design for slug flow in large pipe systems. Also, disturbance waves were observed to be incoherent in large-diameter pipes [17], [18]. In large pipes, the waves were not perpendicular to the flow direction but were localised in curved "bow waves", in contrast to smaller pipes, where the waves are perpendicular to the pipe axis and continuous around the circumference. Omebere-Iyari and Azzopardi [19] provided a quantitative difference between the two pipe scales. They found that Pearce's coeffecient, which is proportional to the film wave velocity, increases with the pipe diameter but maintains a fairly constant value of 0.9 once the diameter reaches 100 mm.

It is evident that inter-phase interactions are different between pipe scales. Nonetheless, the extrapolation of established models obtained using data gathered for small pipes is still widely practiced and can lead to non-optimal design of pipeline systems [20]. We report an experimental

air/water study for a large diameter serpentine pipe facility commissioned by the Oil and Gas Engineering Laboratory at Cranfield University, UK. Data were acquired using a 32×32 capacitance WMS and flush mounted conductance film thickness probes installed at various axial positions after a U-bend to examine the bend's effect on flow development.

2 Experimental setup and procedure

2.1 Flow loop

The air–water two-phase Serpent Rig in the Oil and Gas Engineering Laboratory of Cranfield University is a specially built flow facility that is used in the study of flow behaviour around upward and downward U-bends. As shown in Figure 1, there are three subdivisions: the fluid supply and metering area, the test area, and the separation section. The rig receives measured rates of water and air from the flow metering area to the test rig and finally into the ventilation tank, where the air and water are separated. The water is returned to the storage tank, while the air is vented.

The test area is a flow loop consisting of a system of ABS pipes approximately 20-m long with a 4-inch (101.6-mm) internal diameter. It includes four upward and downward flowing sections connected by three Perspex 180-degree bends. The two middle 6-m vertical pipes are fitted with various instruments to collect data. The right arm of the U is the downward flowing section, which is the area of interest of this study. Compressors fix the pressure rating of the facility and have a maximum discharge pressure of 7 barg, although typical test pressures are around 0.2 to 1 barg.

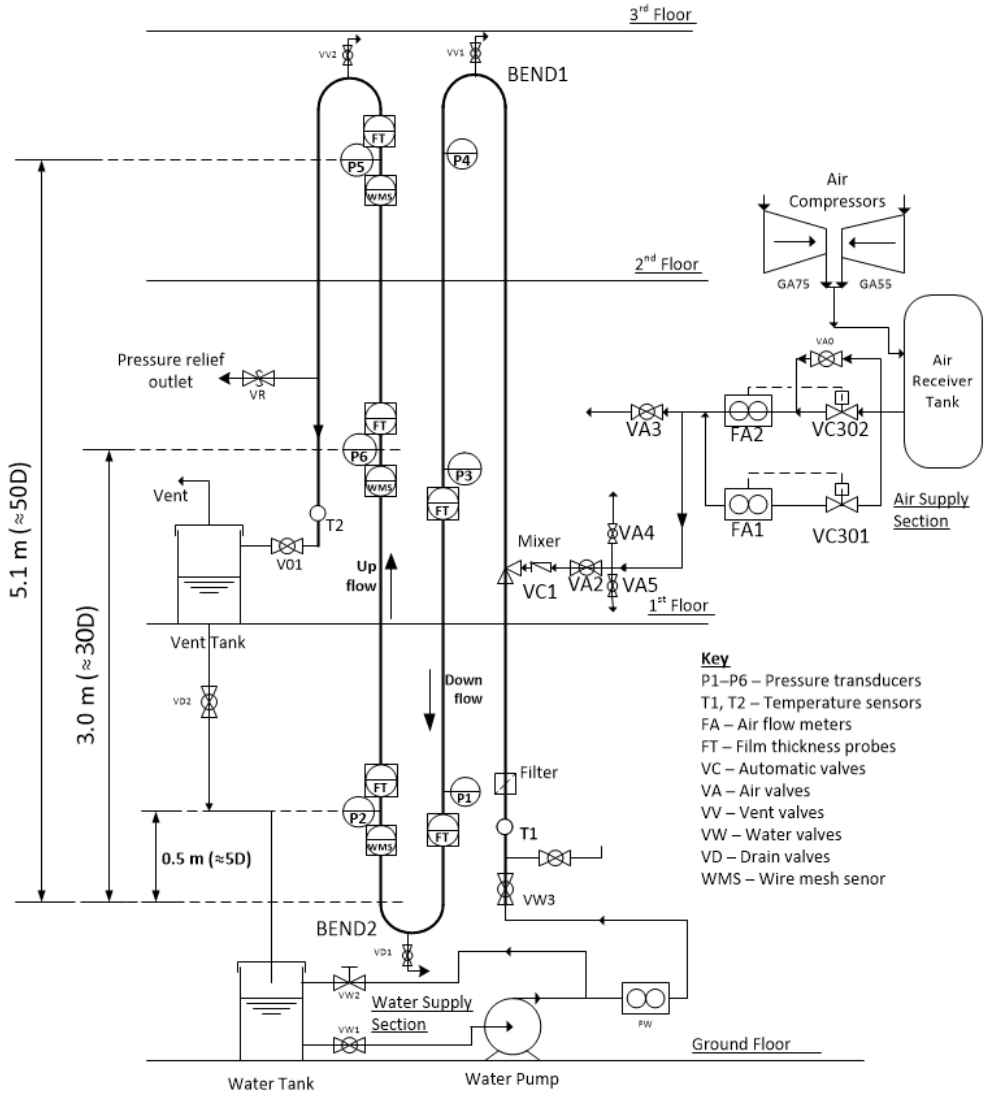

(a) Serpent rig schematic

(b) Bottom section showing return BEND2, viewing section, and instrumentation

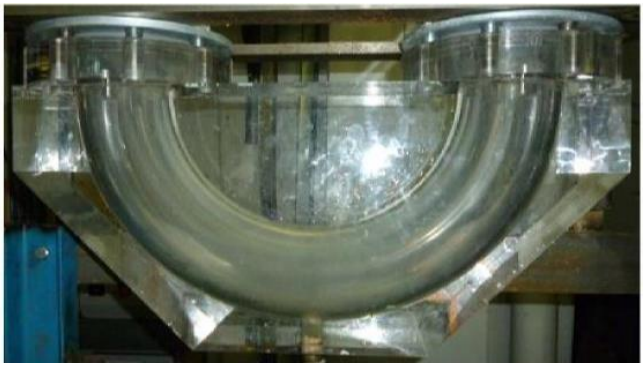

(c) Close up of return BEND2

Figure 1: Air-water serpent rig facility

Air is supplied from a bank of two compressors connected in parallel, GA55 and GA75, which have a combined maximum air flow capacity of 1200 S m^3/h. An 8-m^3 air receiver collects the air from the compressors to dampen fluctuations. Before metering, the air passes through a series of three filters and then through a cooler, where debris and moisture are removed (not shown). The air flow rate is regulated using two automated valves (VC301 and VC302) and measured by either of two Rosemount Mass Probar flow meters (FA1 and FA2). FA1 is used when the air flow rate is within the range of 0–150 S m^3/h ± 0.5%, while FA2 is used when the air flow rate exceeds 150 S m^3/h ± 0.5%.

Water is supplied from a of 1.2-m^3 water tank and transported to the flow loop by a Grundfos CRE3 pump, which delivers variable flow rates and is capable of 26 different speeds. It has a maximum capacity of 10 litres/s ± 0.1% at 6 barg and is metered by a 100-mm ABB electro-magnetic flow meter MMSG-Special. Manual bypass valve VW2 between the pump outlet and the water tank is also used for flow control. For pressure measurements, the facility is equipped with six GE Sensing UNIK 5000 pressure transducers at positions P1–P6 in the downward and upward flowing test sections. The transducers have a range of 0–1.5 bar F.S. Two temperature sensors (range: 0–100° C ± 0.5%) are installed at the entrance and exit of the rig.

2.2 Instrumentation and data acquisition

Wire mesh sensor

The capacitance WMS) was used to measure the cross-sectional void fraction distribution at different axial pipe locations. It has a grid of 32×32 wires and was provided by Helmholtz–Zentrum Dresden–Rossendorf, Dresden, Germany, together with the associated electronics and data processing software. The use of both conductance and capacitance WMSs for measuring phase fractions in gas/liquid flows has been around for over fifteen years since Prasser et al. [21] reported the design of a 16×16 system. It has been validated by several studies for different flow regimes ranging from bubbly to annular flows and for vertical and horizontal pipe orientations [22]–[25].

In the sensor assembly, perpendicular wire electrodes are placed across the cross-sectional area of the flow. One set of the perpendicular wires acts as signal transmitter, while the other acts as a receiver and the wire planes are separated by a small distance with one above the other. The WMS measures the local permittivity of the fluid in the gaps of each grid point by continuously applying an excitation voltage to each sender electrode while keeping others at ground potential and then synchronously measuring the alternating current flow to all receivers. Based on these measurements, the cross-sectional fluid distribution (or void fraction α) across the pipe using the sensor is estimated as follows:

$$\alpha(i,j,k) = \frac{v_l(i,j) - v_{two-phase}(i,j,k)}{v_l(i,j)} \quad (1)$$

where i and j are spatial indices representing the transmitter and receiver wires, respectively ($i = j = 32$ for a 32×32 WMS), and k denotes the frame number, which depends on the frequency and duration of the measurement. $v_l(i,j)$ and $v_{two-phase}(i,j,k)$ are electrical voltage matrices for reference or calibration when the pipe is full of liquid and for instantaneous two-phase situations during experiments.

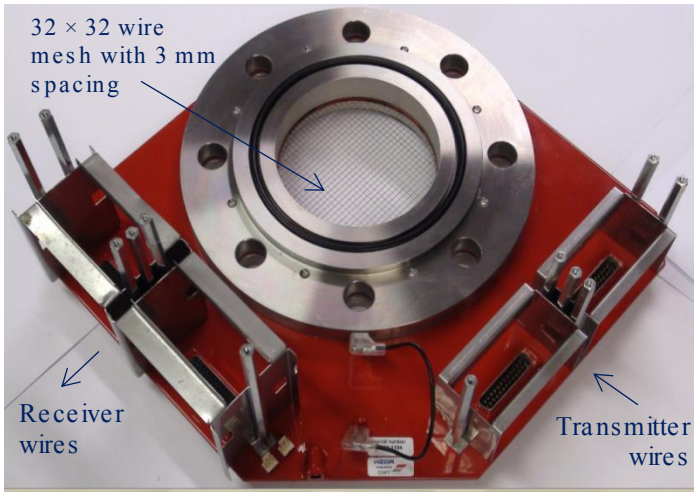

Figure 2: 32×32 capacitance wire mesh sensor

For the sensor used in this study (shown in Figure 2), the separation between the sender and receiver planes of wires is 2.5 mm. The spacing between two wires in parallel is 3.2 mm. A sampling rate of 1000 frames per second was used for the measurements. Validation studies were previously carried out on the measurement accuracy of the system Almabrok et al. [4] and showed errors of around ±10%. Further reading on WMS theory, design, and applications is available elsewhere [8], [21]–[23], [26], [27].

Conductance film thickness probes

The conductance probes used for liquid film thickness measurements in the annular flow regime are shown in Figure 3. It is widely accepted that the normalised output (the ratio of the output voltage to the full scale voltage) should be used for calibration and measurements since it reduces measurement errors due to inconsistent liquid conductivity and other environmental factors, such as temperature. The calibration was done using acrylic blocks of known diameters that were concentrically inserted into the probe spool to form a simulated liquid layer with known thickness. Calibration curves were then plotted against the normalised voltage output obtained offline. Polynomial fits were used in Microsoft Excel to obtain equations for these curves and used to convert online voltages obtained during experiments to film thicknesses. The measurement consistency of the probes is ensured by repeating film thickness measurements, and a standard deviation of 0.1 mm was established. This results in a full-scale error of ±3.3% in the film thickness. Temperature correction

coefficients for the sensors are regularly identified and applied for the correction of errors since conductivity depends on temperature. The correction is applied to a temperature range of 10–35 °C, which covers the two-phase mixture temperature range of 15–26 °C in which the tests were performed. Previous studies were carried out with the film thickness probes and provide detailed descriptions of their design and calibration [4], [28]–[30].

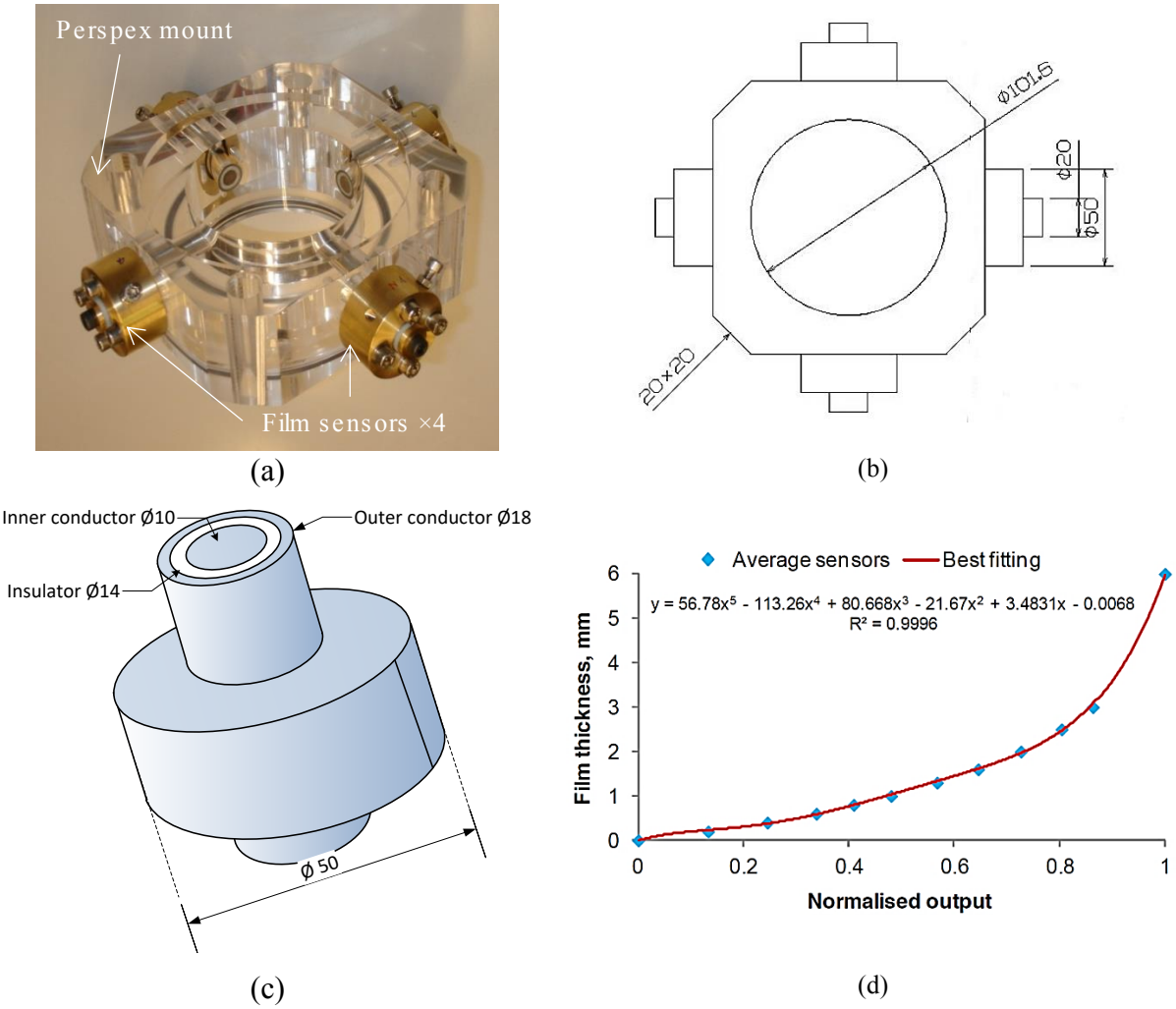

Figure 3: (a) Film thickness sensor spool, (b) Illustration showing dimensions of spool and outer parts of sensor, (c) Details of conducting and insulating parts on the flush side of probe in contact with liquid film, (d) An example of calibration curves used to obtain film thickness from normalised voltage measurements

Data acquisition systems

A DeltaV system and LabVIEW software were used for data acquisition. The DeltaV system records and controls the air flow rates and comes with a fixed sampling rate of 1 Hz, while LabVIEW records the pressures, film thicknesses, and fluid temperatures using a sampling rate of 100 Hz.

3 Experimental results

3.1 Flow regime development in upward flow

Figure 4 shows reconstructed axial images at a fixed superficial velocity (u_{sl} = 1.0) produced by stacking single images temporally captured by the WMS at 1000 fps using a custom program. At lower gas velocities of u_{sg} = 0.53 m/s, the bubbles are generally larger at the top of the pipe due to gas expansion and bubble coalescence. The bubbles are distorted and do not grow large enough to be considered Taylor bubbles, which means the flow regime is not slug flow. This behaviour has been widely reported by earlier investigators working on pipes larger than 100 mm in diameter [7], [12]–[16]. As the superficial gas velocity increases, conditions such as those in the third column of the figure at $u_{sg} = 2.7\ m/s$ dominate the upward flow in the pipe. They are oscillatory and churn-like without a gas continuum in the core of the pipe. Beyond 10 m/s, annular flow occurs. At the bottom position, liquid droplets are entrained in the gas. They decrease in size as they reach the middle of the pipe and seem to disappear as the flow progresses to the top position. It is possible that these droplets are smaller than the 3-mm wire spacing and pass without contacting the wires, which is why they do not register as liquid droplets.

Axial distance from U-bend	$u_{sg} = 0.5\ m/s$	$u_{sg} = 1.0\ m/s$	$u_{sg} = 2.7\ m/s$	$u_{sg} = 18.6\ m/s$
47D	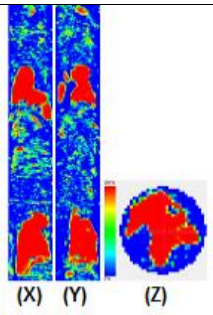	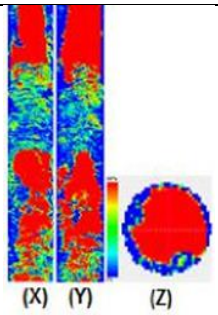	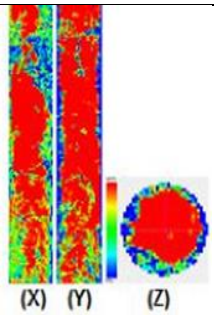	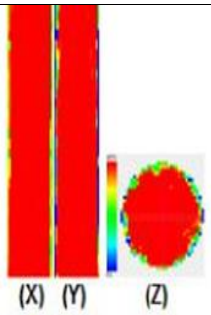
30D	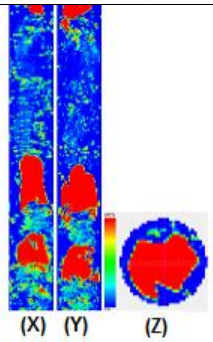	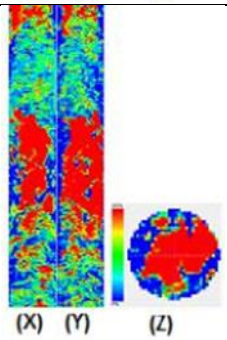	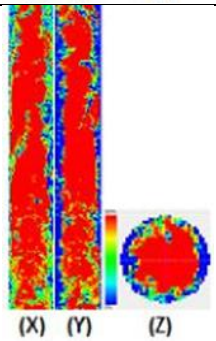	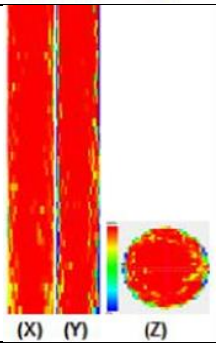

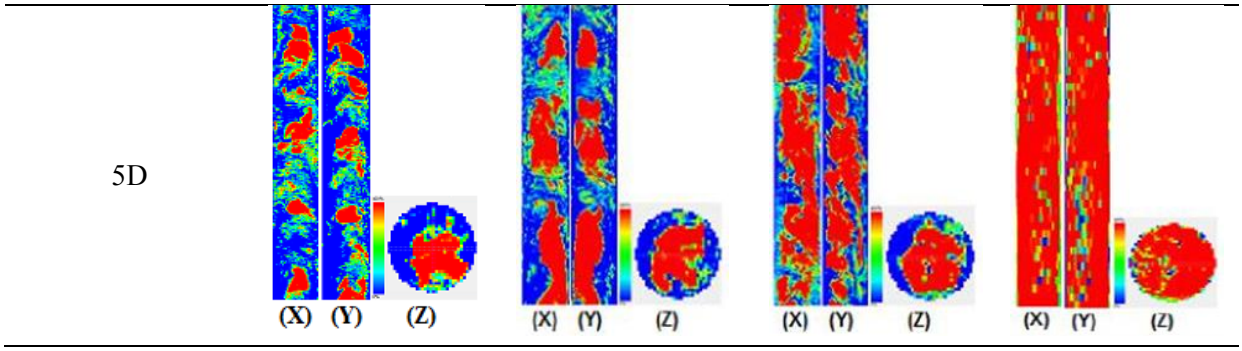

Figure 4: Upflow WMS axial slice and cross-section reconstructed images for phase distribution at different positions for $u_{sl} = 1\ m/s$ at four different u_{sg} values. Blue represents water at 0% void, red represents air at 100% void, and while yellow represents intermediate void fractions (see [28] for more details).

Figure 5 shows the flow visualisation at $u_{sl} = 0.3$ m/s and $u_{sg} = 0.5$ m/s in an unstable flow regime. The unstable regime occurs only at $u_{sl} = 0.2$ and 0.3 m/s up to $u_{sg} = 0.53$ m/s. The WMS shows the occurrence of large bubbles of about ¾ the pipe size. These begin to break down and form a rough and unstable interface but with different characteristics from the traditional churn flow. There is a subtle visual difference in the intermittent flow regime, as shown in Figure 5 (a). However, bubble coalescence occurs downstream (Figure 5 (b) and (c)), and bubbles with more defined interfaces form. These bubbles do not bridge the whole pipe cross section, so the flow cannot be called slug flow. This subtle difference is evident in Figure 4, which compares this occurrence with the same superficial gas velocity of $u_{sg} = 0.5$ m/s and $u_{sl} = 1.0$ m/s.

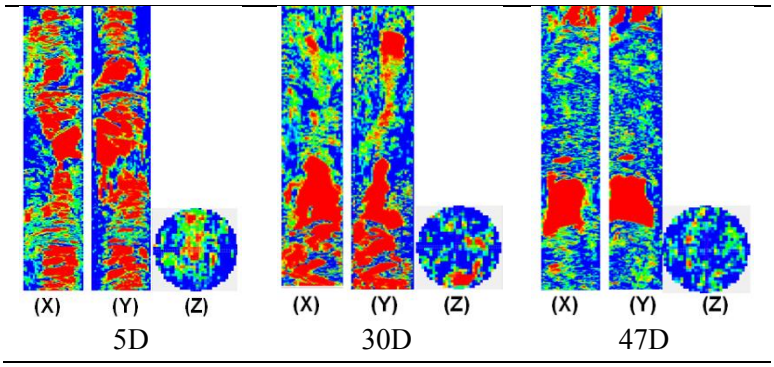

Figure 5: WMS axial reconstructed images at $u_{sl} = 0.3$ m/s and $u_{sg} = 0.5$ m/s showing an unstable flow regime.

Flow patterns identified by both visual observations and reconstructed WMS images are plotted in Figure 6 against the flow regime map from Taitel et al. [31]. They performed many experiments and were able to demarcate where regime transitions occur, which are represented by dashed lines. The transitions are not sharp, and these lines only represent average locations where one regime changes to another, depending on the system pressure, pipe size, and liquid physical properties. Based on our observations, unstable and intermittent patterns dominate. These fall within the slug and

churn regions of the flow map. The figures on the second row occur at $u_{sg} = 1.0\ m/s$ of Figure 4 and continue until around $u_{sg} = 10\ m/s$, from which annular flow occurs regardless of liquid superficial velocity.

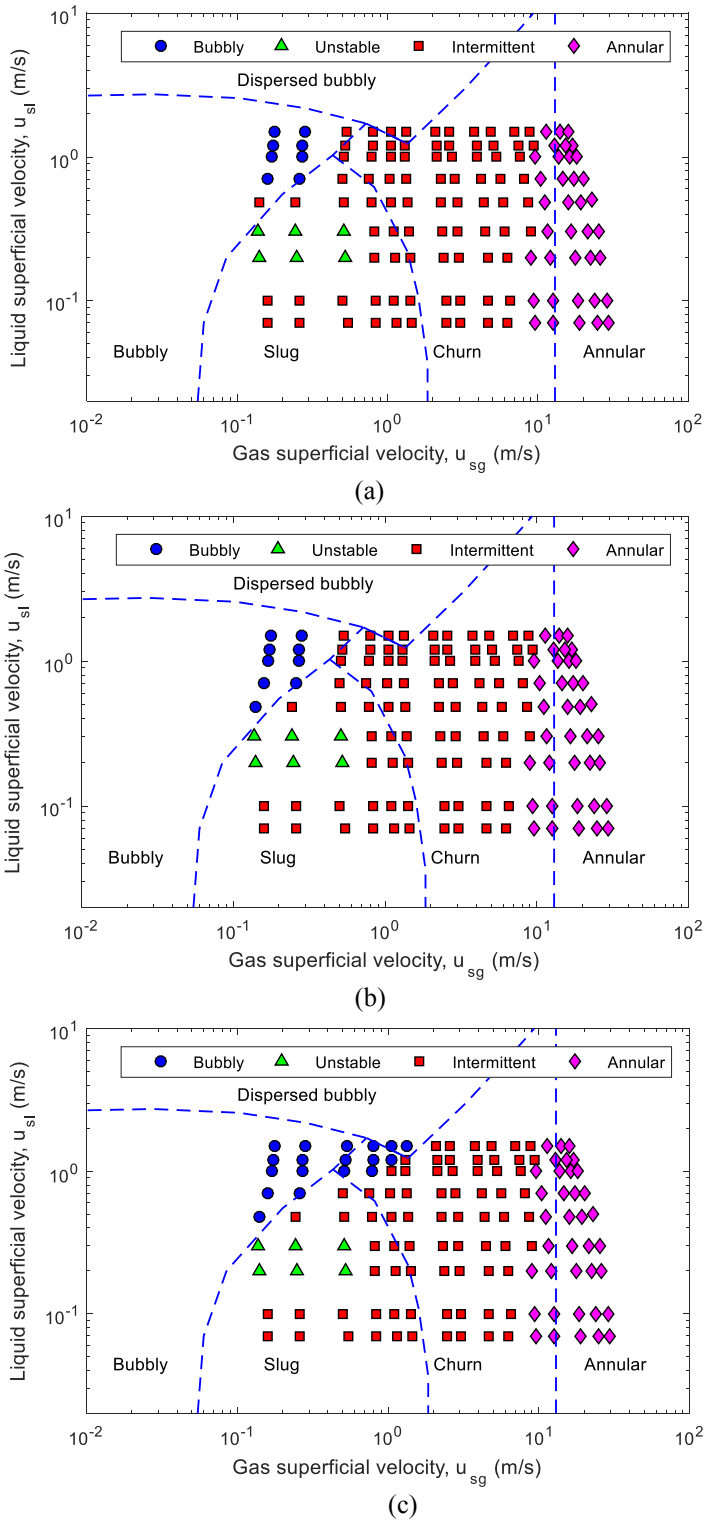

Figure 6: Flow regime maps at (a) top, (b) middle, and (c) bottom position of the upward flowing section after the U-bend. Dashed lines and annotations show the regime transitions based on observations by Taitel et al. (1980) in a 50.8-mm-diameter pipe

3.2 Mean liquid film development

In annular flow, the overall tendency for mean film thickness is to decrease with increasing gas velocity, which is due to some of the liquid on the pipe wall being entrained in the form of droplets in a gas core. This is consistent with the observations obtained in this study. Fukano and Furukawa [32] and MacGillivray and Gabriel [33] suggested that the mean film thickness in fact decreases asymptotically with gas mass flux (or gas superficial velocity) to a minimum regardless of liquid velocity. They partly attributed this asymptotic decrease to the film becoming smoother as the gas superficial velocity increases.

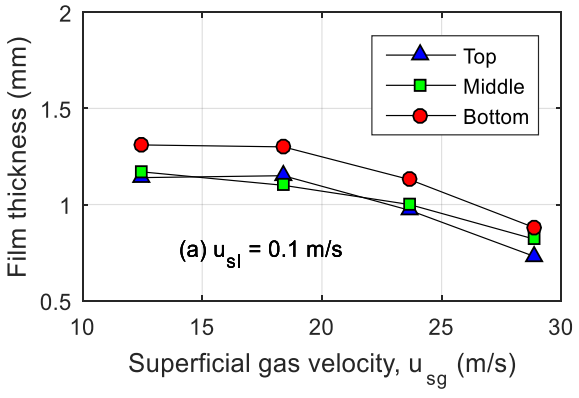

(a)

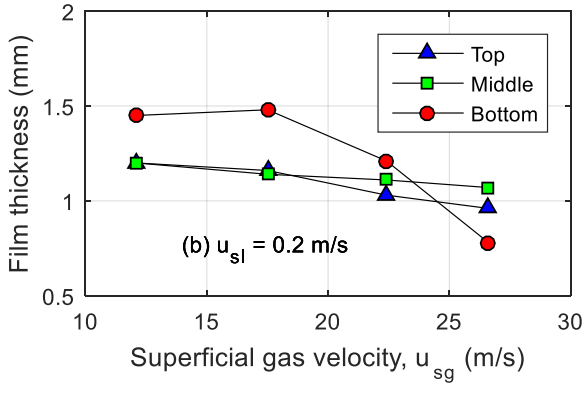

(b)

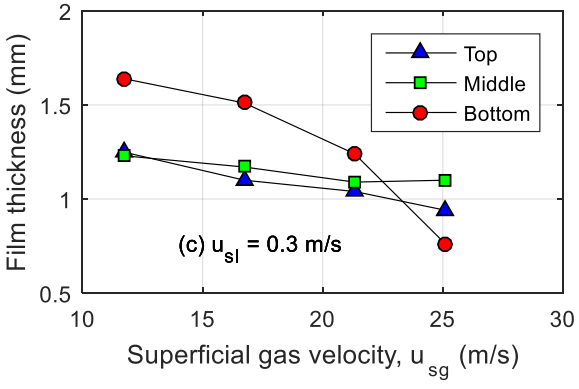

(c)

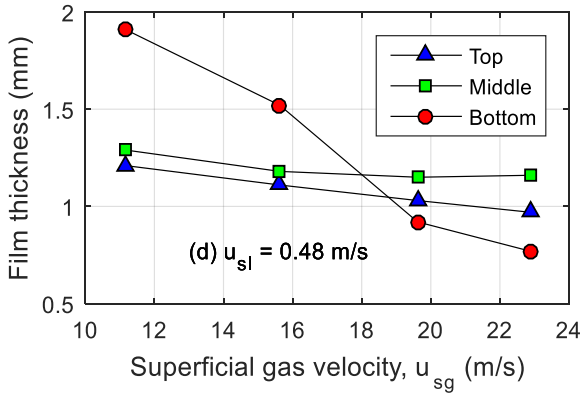

(d)

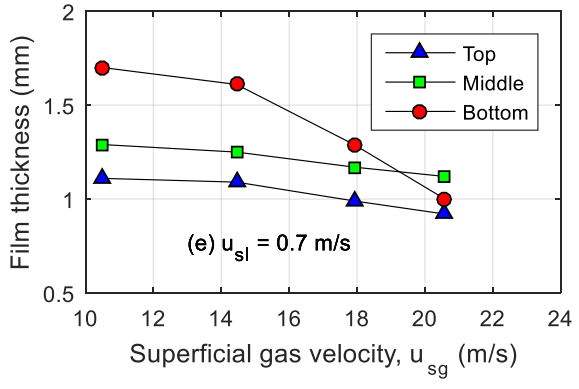

(e)

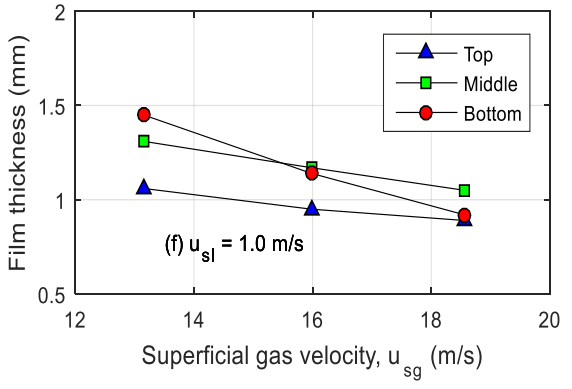

(f)

Figure 7: Effects of gas and liquid superficial velocities on mean film thickness development at the top, middle, and bottom axial positions

Figure 7 (a–f) illustrate the development of the average liquid film thickness versus the superficial air velocities (u_{sg}) at superficial water velocities (u_{sl}) of 0.1–1.0 m/s. For all the plots, the liquid film thickness at the three axial positions (5, 30, and 47 L/D) decrease as u_{sg} increases. The liquid film at the bottom position (at L/D = 5 from the bottom bend) shows a different behaviour at u_{sl} greater than 0.1 m/s. The bend effect becomes more dominant in flow maldistribution as the mixture momentum increases.

The magnitude of the film thickness at the middle and top positions are fairly close to each other for most superficial air velocities, while that at the bottom position is notably thicker. This indicates a fairly developed flow in the middle position of the pipe, and this effect is stronger at higher gas velocities where axial flow development occurs more rapidly. The film thicknesses ratios are defined as the ratio of the film thickness at other L/D positions to that at L/D = 47 (i.e. $t_{ratio} = t/t_{L/D=47}$). This means that t_{ratio} at 47 pipe diameters is unity. There is minimal difference in the mean film thickness ratio between the middle and top positions, thus signifying reasonably stabilised flow. The film thickness ratios at lower superficial gas velocities towards the bottom of the pipe are below 1.5. In contrast, this ratio increases to beyond 1.5 at higher superficial liquid velocities, where the difference between the top and bottom ratios narrow compared to the low liquid velocity conditions. This means that when reaching the middle position of the pipe, the initial bend-disturbed behaviour at the bottom almost completely decays, especially at high liquid superficial velocities.

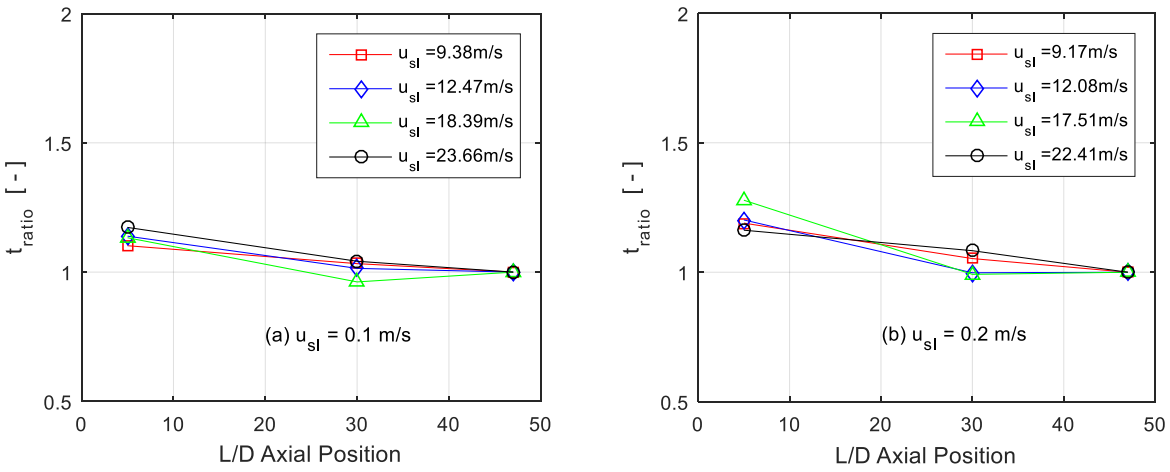

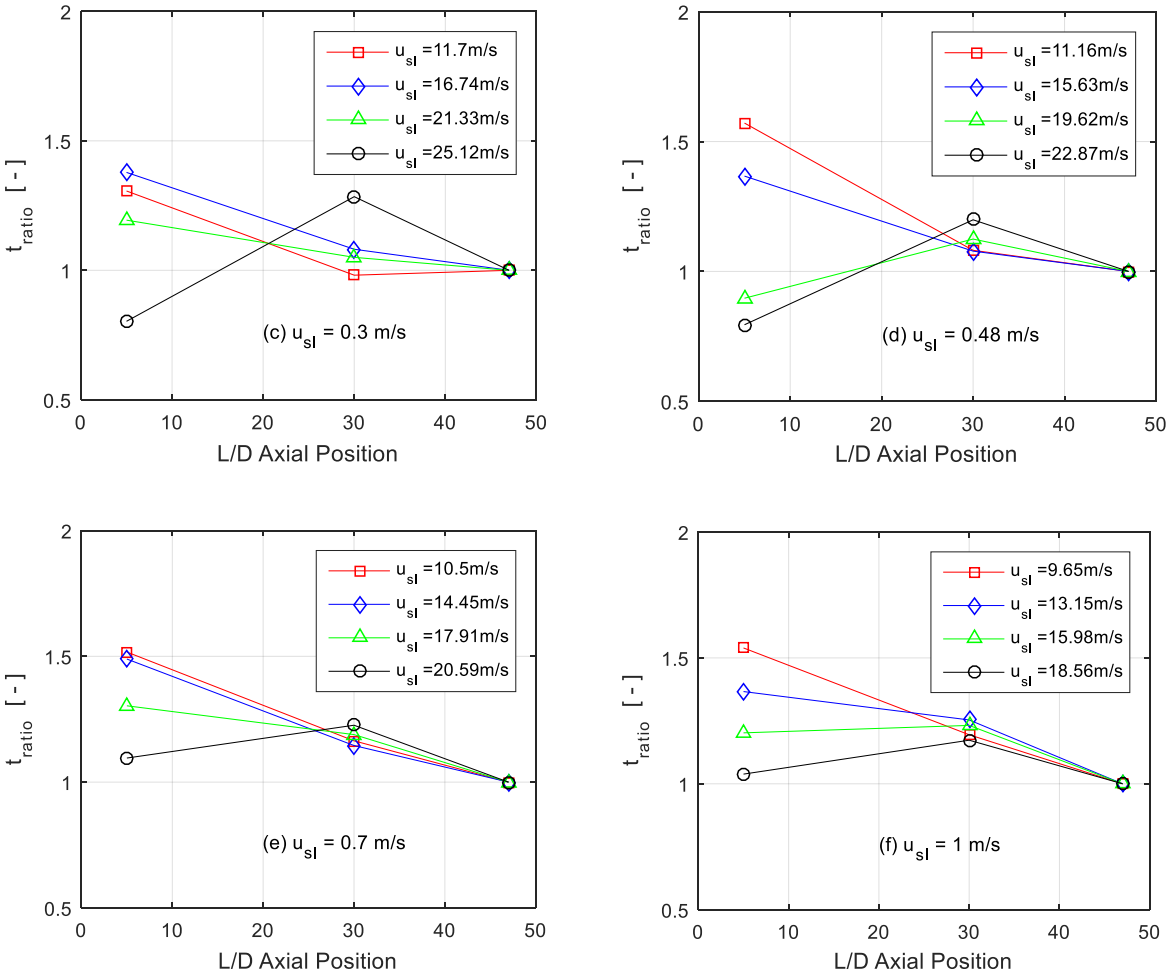

Figure 8: Axial development of the liquid film ratios along the upflow for different superficial air and water velocities.

Both Figures 7 and 8 reveal a reduction in the film thickness along the flow path (from 5 to 47 pipe diameters), even when the superficial air velocity change. Gravity drainage is also more dominant on the liquid than on the gas, and droplet entrainment into the gas core is also responsible for the behaviour. This observation shows good agreement with a previous study [34], in which the film thickness at the pipe inlet increased for a finite distance before decreasing as the flow progressed along the pipe axis. This was firstly attributed to the absence of entrainment near the pipe inlet while the disturbance waves were formed when the flow reached the higher axial locations. These waves are responsible for liquid entrainment phenomenon, resulting in the film thickness starting to decrease. Secondly, the transition between laminar and turbulent flow near the pipe inlet causes the film to be thicker.

3.3 Circumferential distribution of the liquid film

Figure 9 shows the circumferential distribution of liquid film at the top, middle, and bottom positions for fixed superficial water velocities of 0.1, 0.48, and 1.0 m/s at increasing superficial gas velocities for each case of u_{sl}. For the middle and top axial positions, the profiles of the film thicknesses are similar and nearly uniform along the circumference. At the bottom position, however, the film thicknesses are generally thicker and not circumferentially uniform. A thicker water film always occurs at 90° corresponding to the pipe quadrant in the outermost part of the pipe circumference and bend. The near symmetry of the film at the middle and at the top position to a greater extent demonstrates the rapid decay of the centrifugal force acting around the bend as the flow progresses axially. However, there is less level asymmetry for the higher gas and liquid velocities as the mixture momentum gradually dominates the bend's centrifugal force.

u_{sl} = 0.1 m/s	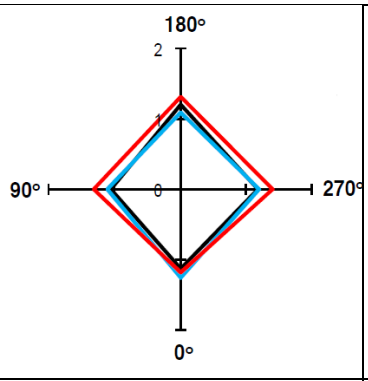	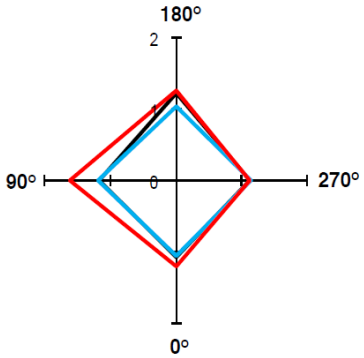	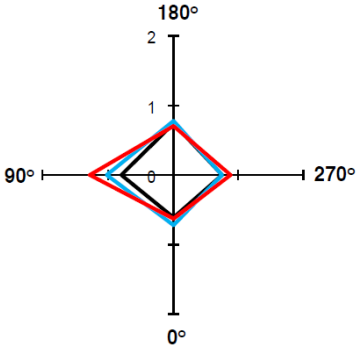
	u_{sg} = 12.5 m/s	u_{sg} = 18.4 m/s	u_{sg} = 28.9 m/s
u_{sl} = 0.48 m/s	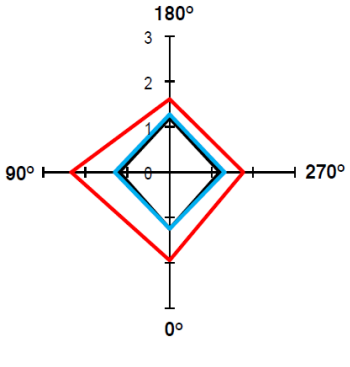	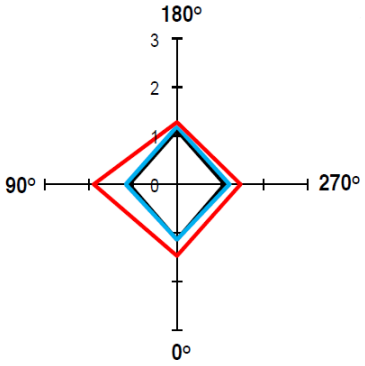	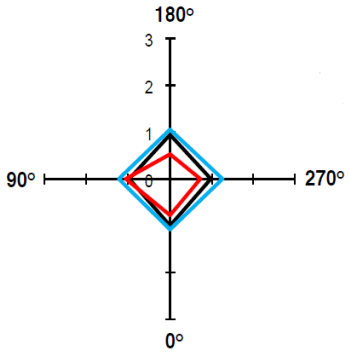
	u_{sg} = 11.6 m/s	u_{sg} = 15.6 m/s	u_{sg} = 22.9 m/s

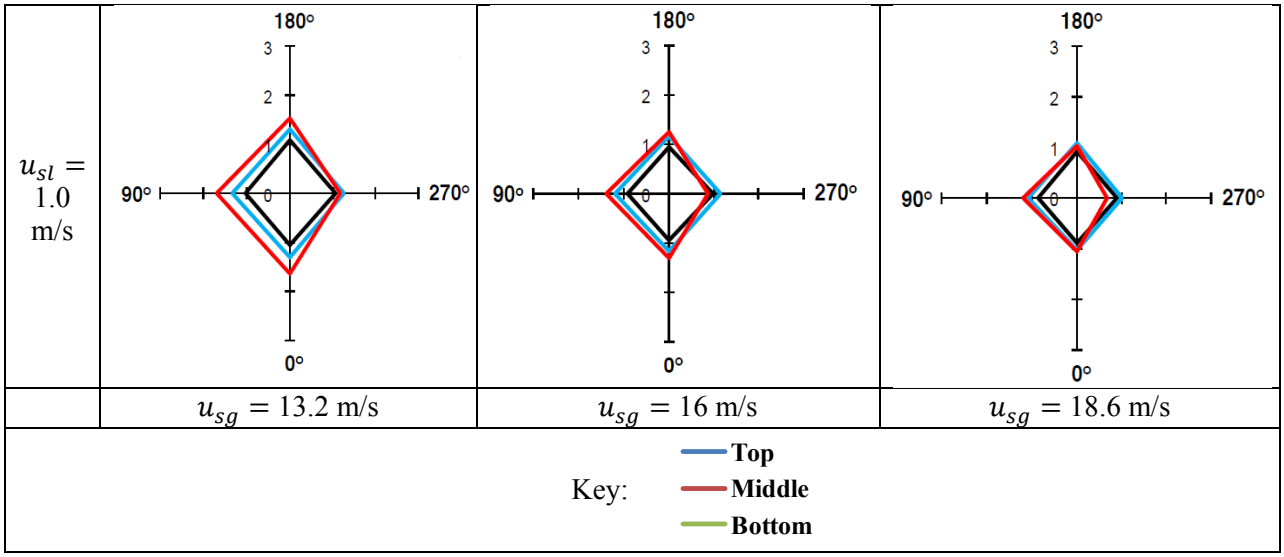

Figure 9: Radar plots showing the effects of gas and liquid superficial velocities on circumferential film thickness variation at the top, middle, and bottom axial positions (u_{sl} = 0.1 m/s; all axis units in mm).

4 Pipe diameter effect on liquid film thickness

Film thickness data from studies on large-diameter pipes have been collected to examine the effect of the pipe diameter on the liquid film thickness in upward annular flows. Such data is scarce because of the large gas and liquid fluxes required to achieve annular flow in large pipes, which make experiments more expensive. Nevertheless, the predictive accuracy of reported models needs to be tested for large pipes to improve pipeline system designs and associated facilities. Correctly predicting film thickness behaviour is particularly crucial in heat transfer applications where dryout situations need to be avoided at all costs.

Knowledge of the critical heat flux becomes important, and the liquid film thickness for each flow condition is therefore indispensable. There are many theoretical and empirical liquid film thickness models for different pipe orientations and fluid combinations, but the overwhelming majority are for pipes with diameters less than 50 mm. However, there is no guarantee that these will be equally successful in larger pipes (>100 mm diameter), where the hydrodynamics are more affected by the pipe scale. For example, applying the conventional one-dimensional drift flux model to large vessels was only limited to low gas flow rates [6]. Azzopardi et al. [17] observed that disturbance waves, which greatly contribute to wall shear stress and droplet entrainment, are circumferentially coherent and uniform in small pipes. However, they were incoherent and localised bow waves in a large-diameter pipe. Quantitatively, Pearce's coefficient, which is proportional to the film disturbance wave velocity, increases with the pipe diameter and maintains a fairly constant value of 0.9 once the pipe diameter crosses 100 mm [19].

4.1 Description of large pipe experimental datasets

Data from this study and published data were thus compared for upward flow film thickness correlations. As shown in Table 1, a total of 65 data points were collected for air–water film thickness in the annular flow regime. The present film measurements were performed using conductance film thickness probes with pressures between 0.9–1.4 bar in a 4-inch (101.6-mm) pipe.

Table 1: Published film thickness data for large-diameter upward annular flow

S/No.	Author(s)	Fluid combination	D (mm)	L/D	Test pressure (bara)	u_{sl} range (m/s)	u_{sg} range (m/s)	Number of data points
1	Zangana [36]	Air/water	127	66	1.0	0.02–1.0	10–17	9
2	Van der Meulen [18]	Air/water	127	87	2.0	0.014–0.04	10–17	22
3	Skopich et al. [35]	Air/water	101.6	58– 92	0.9–1.2	0.01–0.05	14–27	14
4	Current	Air/water	101.6	47	1.0–1.4	0.1-1.0	10–29	20
	Total							65

A wide range of flow regimes was covered in the experiments, and for the comparisons, careful screening was done to select only those that fall in the annular regime (Figure 10). Previous measurements of a liquid holdup in a 101.6-mm riser were also used to study liquid loading phenomena [35]. Those experiments were carried out around atmospheric pressure, and 9 data points in the annular flow regime were used. The final sets of data collected were obtained at pressures of 1 and 2 bar, respectively, in an 11-m riser with 127-mm internal diameter at the University of Nottingham [36] [18].

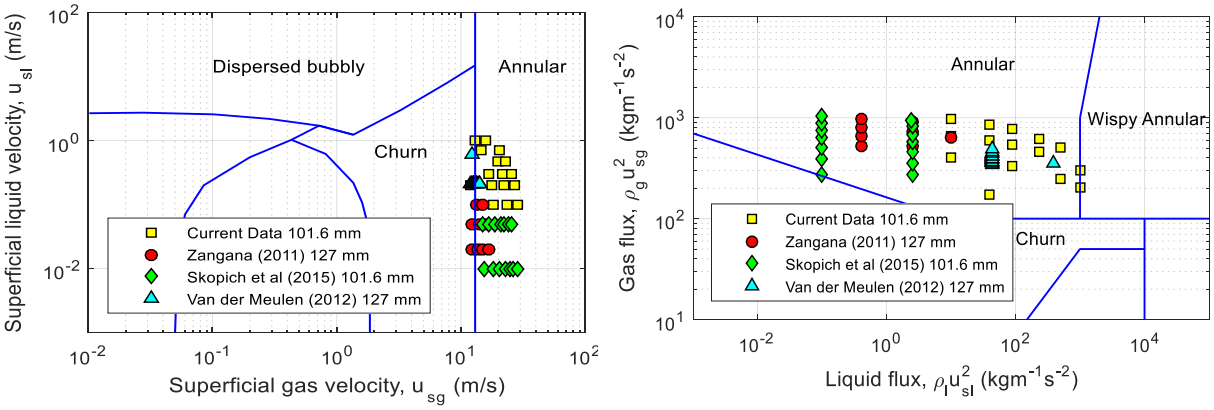

(a) (b)

Figure 10: Experimental datasets against flow regime maps from (a) Y. Taitel, D. Bornea, and A. E. Dukler [31] **and (b) Hewitt and Roberts** [37]**.**

4.2 Film thickness correlations

A class of film thickness models has been theoretically derived from relations describing the velocity profile in the film such as that of Kosky [38] based on Prandtl's 1/7th power law velocity profile within the liquid film:

$$u^+ = 8.74y^{+\frac{1}{7}} \tag{1}$$

where u^+ is the velocity parameter defined as $u^+ = u\sqrt{\rho/\tau}$, u is the liquid film velocity at a distance y^+ from the wall, and τ is the shear stress within the liquid film. y^+ is the friction distance parameter given by $y^+ = (\rho y/\mu)\sqrt{\rho/\tau}$. The mass flow rate per unit wetted perimeter of the thin liquid film is approximated by:

$$\dot{m}_{lf} = \rho_l \int_0^t u\, dy \tag{2}$$

where t is the liquid film thickness. By definition, the liquid film Reynolds number is given as $Re_{lf} = 4\dot{m}_{lf}/\mu_l$. Putting this in Equation (2) yields:

$$Re_{lf} = 4\int_0^t u^+\, dy^+ \tag{3}$$

Substituting Prandtl's 1/7th power law for turbulent films for $Re_{lf} > 1000$ or $t^+ \equiv \left(\frac{\rho t}{\mu}\right)\sqrt{\frac{\rho}{\tau}} > 25$ into Equation (3) gives the model for predicting the dimensionless liquid film thickness explicitly as a function of Re_{lf}:

$$t^+ = 0.0504\, Re_{lf}^{0.875} \tag{4}$$

This is Kosky's film thickness relation, it is considered mechanistic and can in theory be applied irrespective of pipe diameter, but it is still dependent on an empirical velocity profile. Also, the non-dimensional film thickness t^+ in Equation (4) requires pressure gradient measurements in order to determine the shear stress τ, as well as the entrained droplet fraction to calculate the liquid film Reynolds number. In effect, Kosky's equation and others with similar forms are difficult to use since they require iterative solutions of the triangular relationships of film thickness, shear stress τ, and entrained droplet fraction (or liquid film flow rate). Another limitation of using Kosky-type film thickness models is that the effect of the flowing gas is not considered. The flowing gas introduces turbulence at the gas–liquid interface, but Prandtl's 1/7th power law considers only the velocity profile within the liquid film in the absence of external gas interaction.

A modified Martinelli flow parameter was later introduced to eliminate the dependence on τ [39]. The non-dimensionalised film thickness was obtained using the pipe diameter (t/D) rather than the friction velocity (u^+), making the relation explicitly in terms of controlled variables. Introducing the effect of the flowing gas led to the derivation of expressions for the dimensionless film thickness in both downward and upward flows [40]. A characteristic shear stress was introduced, which is the

weighted mean of the wall and interfacial shear stresses ($\tau_c = \frac{2}{3}\tau_w + \frac{1}{3}\tau_i$). Nevertheless, these relationships still rely on the film Reynolds number or the pressure drop measurements. This was also the case for a correlation that expressed the film thickness as t^+ rather than t/D [41], again making it somewhat cumbersome to implement due to its iterative nature and potential convergence problems.

Other authors have avoided these pitfalls by directly correlating t/D with functions of dimensionless quantities such as the Reynolds, Froude, Weber, or viscosity numbers, the density/viscosity ratios, and the gas quality x. Table 2 summarizes the liquid film thickness correlations for upward gas–liquid two-phase flow. The correlating procedure is achieved by curve-fitting a large amount of data using nonlinear regression techniques. Attempts have been made to incorporate the effect of pipe diameter by developing correlations using film thicknesses from experiments in pipes of different sizes, but these are still limited to channels of less than 3 inches (76 mm) in size. Examples include pipes of 13.0, 19.8, and 26.1-mm diameter [42] and 8.8–50.8-mm diameter [43]–[47].

Table 2: Film thickness correlations considered in this study

Author(s)	Equation	Remarks
Henstock and Hanratty [39]	$\frac{t}{D} = \frac{6.59F}{(1+1400F)^{0.5}}$, where $F = \frac{0.0379Re_l^{0.9}}{Re_g^{0.9}}\frac{\nu_l}{\nu_g}\sqrt{\frac{\rho_l}{\rho_g}}$	Semi-empirical, basis is momentum/static force balance on the liquid film, used both vertically up and downward data from 7 studies with pipe diameters of 12–64 mm.
Hori et al. [42]	$\frac{t}{D} = 0.905Re_g^{-1.45}Re_l^{0.90}Fr_g^{0.93}Fr_l^{-0.68}\left(\frac{\mu_l}{\mu_{l,ref}}\right)^{1.06}$	Empirical, used air/glycerol data from pipes of 13–26 mm diameter. Noted that film thicknesses so obtained were larger than those of more viscid liquid systems
Fukano and Furukawa [32]	$\frac{t}{D} = 0.0594\exp\left(-0.34Re_l^{0.19}Fr_g^{0.25}x^{0.6}\right)$, where $x = \frac{\rho_g u_{sg}}{\rho_g u_{sg}+\rho_l u_{sl}}$	Empirical, effect of viscosity was studied by using air/water, air/glycerol solutions in 26 mm pipe.
MacGillivray [44]	$\frac{\rho_l u_{sl} t}{\mu_l} = 39Re_l^{0.2}\left(\frac{1-x}{x}\right)\left(\frac{\rho_g}{\rho_l}\right)^{0.5}$	Empirical, air and helium/water experiments conducted in normal, micro, and hyper-gravity in 9.5 mm pipe. Liquid superficial velocities were 0.09–0.3 m/s while gas velocities ranged between 18 and 79 m/s. Double-wire conductance probes were used for film measurements.
Berna et al. [43]	$\frac{t}{D} = 7.165Re_g^{-1.07}Re_l^{0.48}\left(\frac{Fr_g}{Fr_l}\right)^{0.24}$	Empirical, utilised data from 5 studies including those of [53]–[55] involving both vertical and horizontal flow in pipes of 8.8–50.8 mm diameter.
Ju et al. [45]	$\frac{t}{t_{max}} = tanh\left(14.22We_l^{0.24}We_g''^{-0.47}N_{\mu_l}^{0.21}\right)$ where $We_g'' = \frac{\rho_g u_{sg}^2 D}{\sigma}\left(\frac{\Delta\rho}{\rho_g}\right)^{0.25}$, and $N_{\mu_l} = \frac{\mu_l}{\sqrt{\rho_l\sigma\sqrt{\frac{\sigma}{g\Delta\rho}}}}$, and $t_{max} = 0.06D$	Empirical, used over 350 data points from the air/water studies of [32], [46], [47], at 1–6 bar pressure ranges, pipe diameters of 9–32 mm, and gas velocities of 15–100 m/s.

Investigators have also produced correlations with data involving liquids with differing viscosities. Examples used 0.001, 0.005, and 0.01 Pa.s glycerol solutions [42] and experiments conducted using four liquid viscosities from 0.008–0.00997 Pa.s corresponding to glycerol in different concentrations: 0% aqueous glycerol solution (pure water), 45% aqueous glycerol solution, 53% aqueous glycerol solution, and 60% aqueous glycerol solution [32]. As shown in Figure 11, these correlations describe the large-pipe database with varying degrees of success. Figure 11 (a) shows the prediction of Henstock and Hanratty's correlation compared with the experimental film thicknesses. Superficial quantities were used in the calculation of the Reynolds numbers in the absence of the film flow rate, which gives good predictions. Most of the values fall within a ±30% error band, suggesting that the modified Martinelli flow parameter is equally applicable in large channel flow. However, the validity appears to be limited to $u_{sl} > 0.3\, m/s$, where the films are thicker than $t/D = 0.015$ and over-predictions beyond the ±70% error region occur.

Other correlations also provide reasonable results [32], [42]–[44]. Over 90% of their predictions are within the ±70% error band with the exception of the Fukano and Furukawa correlation, for which only 49% are within this band. The worse predictions were made for the present data and that of Van der Meulen. Fukano and Furukawa's correlation was produced with film thicknesses obtained in only one pipe diameter of 26.1 mm, despite its ability to capture a range of liquid viscosities. The current dataset and that of Van der Meulen use water at room temperature and hence give a single liquid viscosity, so the correlation is not expected to have a significant effect with respect to viscosity in these cases. Also, the development length of their experiments is 133, meaning entrance effects do not affect the efficacy of the correlation

Other equations [42], [43] provided similar predictions (see Figure 11 (b) and (e)), which is not surprising given the similarity in their choice and indices of dimensionless numbers (gas/liquid Reynolds and Froude numbers). As shown in Table 3, the two correlations produced 26.6% and 22.9% mean absolute deviation, respectively, which is defined as follows:

$$MAD = \frac{1}{n}\sum_{1}^{n}\frac{\left|t_{exp} - t_{model}\right|}{t_{exp}} \times 100\% \quad (5)$$

where n is the number of data points, and the subscript exp denotes experimental data. For the correlations of Hori et al. and Berna et al., 63.2% and 64.8% of their predictions were within the ±30% error band, while 96.3% and 93.8% of their film thicknesses were within the ±70% error band, respectively. Figure 11 (f) shows a comparison of another correlation [45] and the large-pipe experimental database. The correlation was developed using over 350 data points from air/water studies [32], [46], [47] at pressure of 1–6 bar with pipe diameters of 9–32 mm and gas velocities of 15–100 m/s. The correlating parameters are a densimetric Weber number and a modified viscosity number. The non-dimensional film thickness was calculated using a maximum film thickness

obtained by solving a transition criterion [48] that was thought to be produced at the inception of annular flow. For diameter ranges of 5–250 mm and pressure changes from 1 to 10 bar, a certain function of the void fraction at the transition changes by less than 5%. Hence, the maximum film thickness was estimated as 0.06D. Under-predictions are produced in small t/D regions by this correlation, while progressive over-predictions occur as the films become thicker. However, only about 7% of all predicted points fall outside the +70% error line.

MacGillivray [44] proposed a correlation for the liquid film thickness in vertical annular flow. Air/helium and air/water experiments were conducted in normal-, micro-, and hyper-gravity in a 9.5-mm pipe. The liquid superficial velocities were 0.09–0.3 m/s, while gas velocities ranged from 18 to 79 m/s. Double-wire conductance probes were used for the film measurements. Despite the 9.5-mm pipe, which is comparatively small even for macro-scale small-diameter pipe studies, the correlation showed remarkable performance against the large pipe database in this study, with all predictions falling within the ±70% error band. MacGillivray non-dimensionalised his film thickness using a film Reynolds number that utilises the superficial liquid velocity and correlated it with the liquid Reynolds number, functions of the gas quality, and fluid density ratios. Only 55.2% of the points are within the ±70% error limit, giving a MAD of 36.3%. However, the point distribution shown in Figure 11 (d) does not produce the deviations at large film thicknesses that occur for other correlations. As such, this correlation appears to be the best overall performer among those surveyed. In light of this, a modified MacGillivray correlation was obtained as follows:

$$\frac{\rho_l u_{sl} t}{\mu_l} = 0.02 Re_l^{0.72} \left(\frac{1-x}{x}\right)^{0.5} \left(\frac{\rho_l}{\rho_g}\right)^{0.08} \tag{6}$$

where $Re_l = \rho_l u_{sl} D/\mu_l$, and $x = \rho_g u_{sg}/(\rho_g u_{sg} + \rho_l u_{sl})$. Figure 12 shows a plot of this equation's predicted points against the large pipe experimental film thicknesses. Most of the points lie within the ±30% error limit. As shown in Table 3, Equation (6) produces considerably improved predictions of the large pipe film thickness database compared to the existing correlations, with 92.4% of all predictions within ±30% of the experiments. In comparison, for one correlation [39], only 71.1% of the points were in this error band. Also, our modified McGillivray correlation produces the lowest MAD of 14.3%.

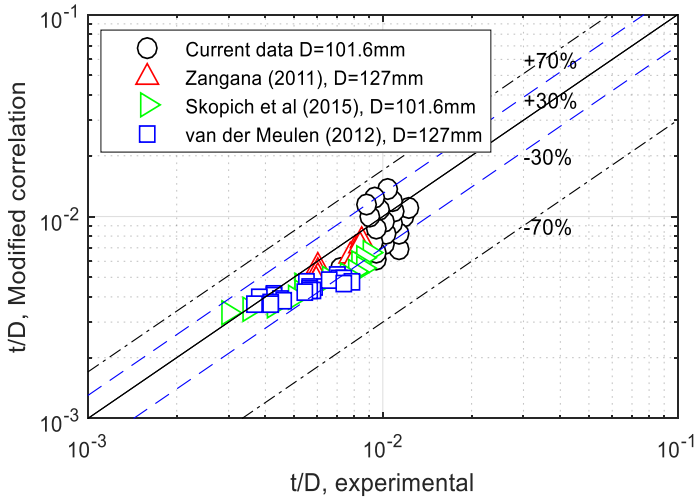

Figure 11: Comparison of predictions by new correlation with large pipe dimensionless liquid film thicknesses

Table 3: Comparison of individual large diameter dimensionless film thickness datasets with predictions of present correlation and select previous correlations

Film thickness data source \ Correlation		Henstock and Hanratty [39]	Hori et al. [42]	Fukano and Furukawa [32]	Macgillivray [44]	Berna et al. [43]	Ju et al. [45]	Present (Eqn (6))
MAD [%]	Current data	51.9	31.6	124.4	40.4	28.8	48.0	13.0
	Zangana [36]	16.5	9.7	72.8	42.4	7.4	24.9	6.9
	Skopich et al. [35]	21.9	18.3	25.8	48.0	18.8	50.4	22.1
	Van der Meulen [18]	9.0	47.0	104.7	14.5	36.6	40.6	15.2
	Overall	24.8	26.6	81.9	36.3	22.9	41.0	14.3
% of predictions within 30% error band	Current data	35.0	60.0	20.0	30.0	65.0	40.0	100.0
	Zangana [36]	77.8	100.0	0.0	100.0	100.0	55.6	100.0
	Skopich et al. [35]	71.4	92.9	57.1	0.0	71.4	0.0	78.6
	Van der Meulen [18]	100.0	0.0	0.0	90.9	22.7	0.0	90.9
	Overall	71.1	63.2	19.3	55.2	64.8	23.9	92.4
% of predictions within 70% error band	Current data	70.0	85.0	30.0	100.0	90.0	75.0	100.0
	Zangana [36]	100.0	100.0	55.6	100.0	100.0	100.0	100.0
	Skopich et al. [35]	100.0	100.0	100.0	100.0	100.0	100.0	100.0
	Van der Meulen [18]	100.0	100.0	9.1	100.0	100.0	100.0	100.0
	Overall	92.5	96.3	48.7	100.0	97.5	93.8	100.0

Figure 13 visually summarizes the information in Table 3 and shows how the correlations perform against the experimental databank. Figure 13 (a) shows that Fukano and Fukano's correlation produced the highest MAD with just over 80%, while the other values were below 40% with the present correlation giving the lowest value. Similarly, Figure 13 (b) and (c) show that the present correlation and that of Henstock and Hanratty were the best performing in terms of the number of

mean film thickness predictions within the ±30% and ±70% error limits. That of Fukano and Furukawa was again the least successful.

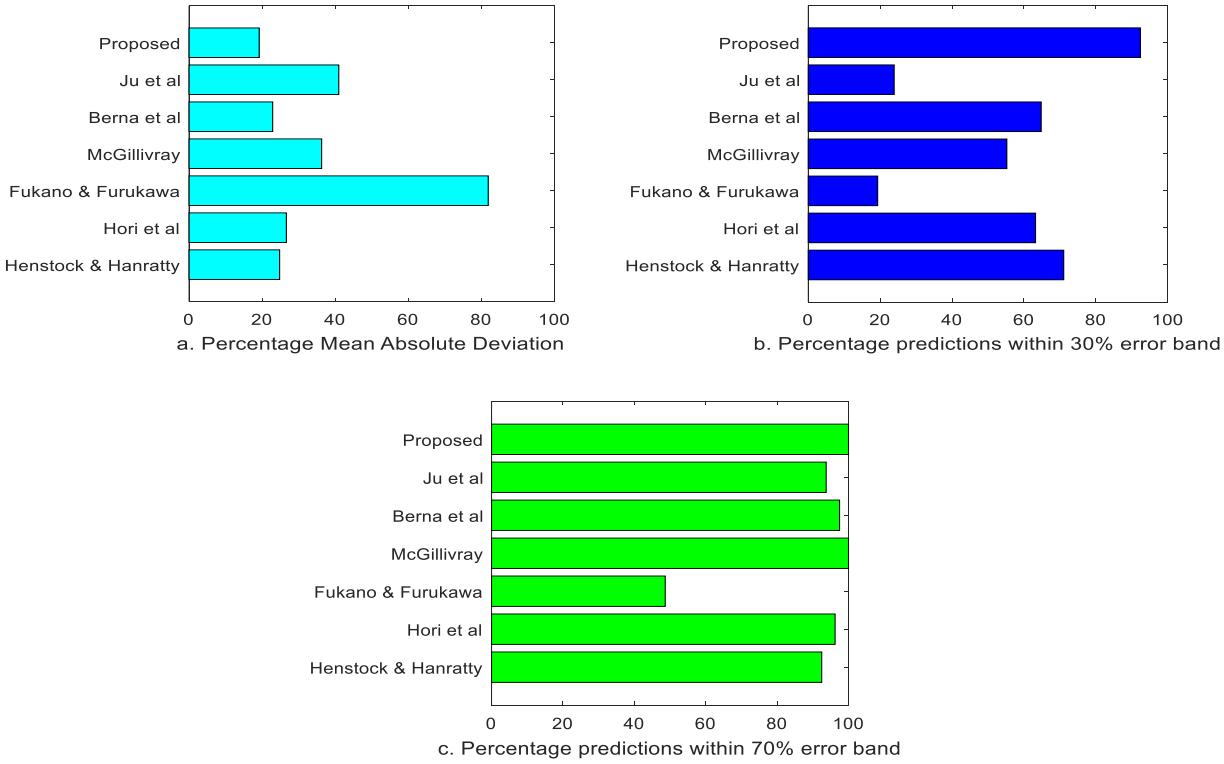

Figure 12: Bar charts showing comparison between the non-dimensional film thicknesses predictions of proposed and previous correlations against the respective datasets

Generally, the mean film thickness has an inverse relationship with the gas velocity. Previous investigators [32], [45] have derived exponential and hyperbolic tangent decay relationships, respectively. Figure 13 (a)–(d) show the proposed correlation's predictions of film thickness between superficial gas velocities of 10 and 100 m/s. It exhibits an inverse relationship and an ability to adjust to the liquid velocity, system pressure, and pipe diameter. The previous data [18], [35], [36] show good agreement at low superficial liquid velocities of between 0.01–0.05 m/s, while the current data, which gave higher film thicknesses due to the larger liquid flow rates, showed that the correlation also gives excellent predictions at higher liquid flow.

However, it appears that the dimensionless film thickness in smaller-diameter pipes results in a much steeper slope with increasing gas velocity, as shown in Figure 13 (e) for t/D from previous works [49]–[52] with 50, 23.4, 50, and 5-mm pipes. The film thicknesses decrease much faster with u_{sg}, despite having thicker films at low gas flow conditions. Higher turbulence in the confined smaller channels may contribute to increased droplet entrainment and hence thinner films than in large pipes. The implication for heat transfer applications is that dryout is more likely to occur more quickly in smaller pipes than in large diameter at similar superficial gas/vapour velocities. For design

purposes, larger conduits should thus be chosen when possible, although this may incur larger capital costs. Therefore, trade-offs may be involved in order to select the optimal pipe size for dryout prevention to achieve the heat transfer objective within a permitted capital cost target.

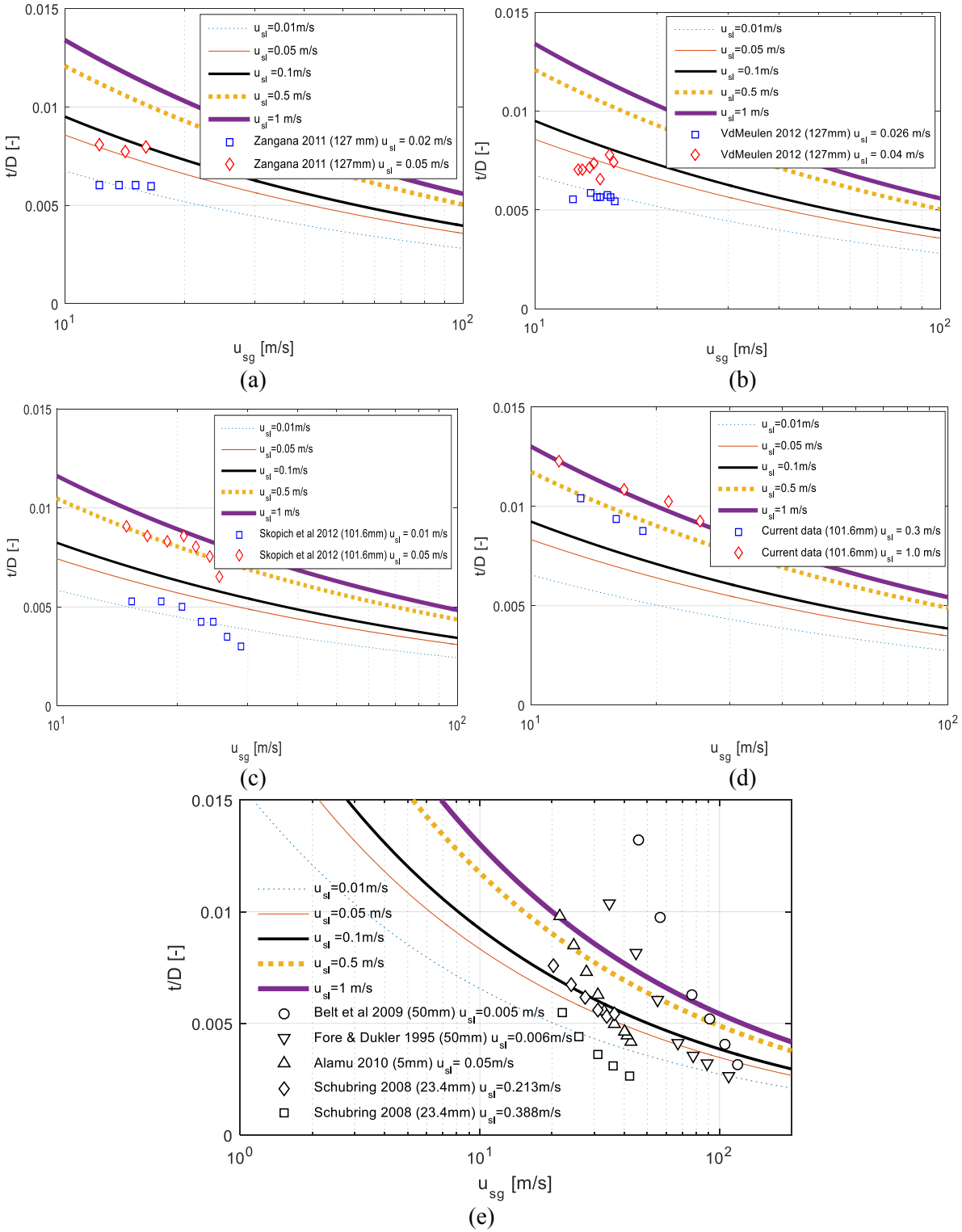

Figure 13: Sensitivity of correlation to system pressure and pipe diameter. Film thickness data of (a) Zangana [36] **at 2-bar pressure, 127-mm pipe diameter, (b) Van der Meulen** [18] **at 2-bar pressure, 127 mm, (c) Skopich et al.** [35] **at 1 bar, 101.6 mm, (d) Current data at 1-1.4 bar pressure, (e) Selected small pipe studies. Lines are predictions by the new correlation at the stated liquid superficial velocities.**

5 Conclusions

We reported an experimental study of the flow development in a vertical pipe section downstream of a U-bend in a pipe with a large diameter of 101.6 mm in a serpentine configuration. A capacitance WMS was used for flow visualisation to help distinguish flow regimes. We presented reconstructions from temporally acquired images at the bottom, middle, and top positions of the pipe. A spool containing four conductance film thickness probes was used to examine the film thickness development in annular flow at 5, 30, and 47 pipe diameters from the U-bend. The conclusions are summarised as follows:

1. The two-phase flow downstream of the U-bend stabilised when reaching 30 pipe diameters. Cross-sectional film thicknesses at this position were already symmetrical and remarkably similar to those obtained at 47 pipe diameters, especially at high liquid and gas velocities (in the annular regime). Also, in these conditions, the magnitude and ratio of the film thicknesses were within 5% of each other in both the middle and top positions, signifying reasonable flow development.
2. Large-diameter pipe film thickness data were collected from published sources and used with those collected in the current study to test the accuracy of existing predictive correlations derived from flow in pipes of small diameter. The predictions exhibited increasing deviation when compared to the large-pipe experimental film thicknesses, which was more pronounced at large values of dimensionless film thickness t/D near conditions at the inception of annular flow.
3. The best performing correlation [44] was modified to improve the dimensionless film thickness prediction. Together with several film thickness data from pipes of 50 mm diameter and below, it was shown that film thickness in large-diameter pipes is less sensitive to increased gas flow at all liquid flow rates than in small-diameter pipes. This may occur because increased turbulence intensity in small pipes promotes droplet entrainment, resulting in thinner films in relation to the diameter as the gas velocity increases in such pipes.

6 Acknowledgement

AMA and YDB would like to express sincere gratitude to the Nigerian Government for funding their PhDs through the Petroleum Technology Development Fund's Overseas Scholarship Scheme (PTDF/E/OSS/PHD/AMA/622/12 and PTDF/E/OSS/PHD/BYD/532/12, respectively). AAA would like to thank the Libyan Government for funding his PhD. This work was also supported by the National Research Foundation of Korea (NRF) grant funded by the Korean government (MSIP) through GCRC-SOP (No. 2011-0030013). We also acknowledge the funding provided by the BK21 Plus Program of the School of Mechanical Engineering, Pusan National University, Republic of Korea. Finally, for data processing, image reconstruction software, and technical support, we thank

Prof. Hampel and his group at Helmholtz-Zentrum Dresden-Rossendorf, Germany, as well as Prof. Da Silva and his group at Universidade Tecnológica Federal do Paraná, Brazil.

7 Nomenclature

A. Roman

A	[m^2]	Cross-sectional area
D	[m]	Pipe internal diameter
e	[-]	Entrained liquid fraction
Fr	[-]	Froude number
g	[m/s^2]	Acceleration due to gravity
G	[kg/m^2-s]	Total liquid mass flux
L	[m]	Pipe length
$\dot{m}$	[kg/s]	Phase mass flow rate
P	[Pa]	Local pressure
Re	[-]	Reynolds number
t	[m]	Film thickness
u	[m/s]	Phase velocity as specified by subscript
u^+	[-]	Velocity parameter
We	[-]	Weber number
x	[-]	Gas quality
y^+	[-]	Friction distance parameter

B. Greek

ε	[-]	Void fraction
γ	[-]	Liquid droplet hold up
μ	[kg/s-m]	Dynamic viscosity
ρ	[kg/m^3]	Density
σ	[N/m]	Liquid surface tension

C. Subscripts

g	Gas phase
l	Liquid phase
lf	Liquid film
sg	Superficial gas
sl	Superficial liquid

8 References

[1] G. H. Anderson and P. D. Hills, “Two-phase annular flow in tube bends,” in *Symposium on Multiphase Flow Systems*, 1974.

[2] T. Oshinowo and M. E. Charles, “Vertical two-phase flow part I. Flow pattern correlations,” *Can. J. Chem. Eng.*, vol. 52, no. 1, pp. 25–35, Feb. 1974.

[3] M. Abdulkadir, D. Zhao, A. Azzi, I. S. Lowndes, and B. J. Azzopardi, “Two-phase air-water

flow through a large diameter vertical 180 o return bend," *Chem. Eng. Sci.*, vol. 79, pp. 138–152, 2012.

[4] A. A. Almabrok, A. M. Aliyu, L. Lao, and H. Yeung, "Gas/liquid flow behaviours in a downward section of large diameter vertical serpentine pipes," *Int. J. Multiph. Flow*, vol. 78, pp. 25–43, 2016.

[5] R. V. A. Oliemans, B. F. M. F. M. Pots, and N. Trompé, "Modelling of annular dispersed two-phase flow in vertical pipes," *Int. J. Multiph. Flow*, vol. 12, no. 5, pp. 711–732, Sep. 1986.

[6] I. Kataoka and M. Ishii, "Drift flux model for large diameter pipe and new correlation for pool void fraction," *Int. J. Heat Mass Transf.*, vol. 30, no. 9, pp. 1927–1939, Sep. 1987.

[7] N. K. Omebere-Iyari, "The effect of pipe diameter and pressure in vertical two-phase flow," University of Nottingham, 2006.

[8] N. K. Omebere-iyari, B. J. Azzopardi, D. Lucas, M. Beyer, and H. Prasser, "The characteristics of gas / liquid flow in large risers at high pressures," vol. 34, pp. 461–476, 2008.

[9] R. Kaji and B. J. Azzopardi, "The effect of pipe diameter on the structure of gas / liquid flow in vertical pipes," *Int. J. Multiph. Flow*, vol. 36, no. 4, pp. 303–313, 2010.

[10] D. J. Peng, M. Ahmad, C. P. Hale, O. K. Matar, and G. F. Hewitt, "Flow regime transitions in large diameter pipes," in *7th International Conference on Multiphase Flow (Multiphase 7)*, 2010, pp. 1–9.

[11] L. Lao, L. Xing, and H. Yeung, "Behaviours of elongated bubbles in a large diameter riser," in *8th North American Conference on Multiphase Technology (Multiphase 8)*, 2012, no. 1998, pp. 381–392.

[12] J. P. Schlegel, S. Miwa, S. Chen, T. Hibiki, and M. Ishii, "Experimental study of two-phase flow structure in large diameter pipes," *Exp. Therm. Fluid Sci.*, vol. 41, no. 2012, pp. 12–22, Sep. 2012.

[13] T. R. Smith, J. P. Schlegel, T. Hibiki, and M. Ishii, "Two-phase flow structure in large diameter pipes," *Int. J. Heat Fluid Flow*, vol. 33, no. 1, pp. 156–167, Feb. 2012.

[14] H. Cheng, J. H. Hills, and B. J. Azzorpardi, "A study of the bubble-to-slug transition in vertical gas-liquid flow in columns of different diameter," *Int. J. Multiph. Flow*, vol. 24, no. 3, pp. 431–452, 1998.

[15] A. Ohnuki and H. Akimoto, "Experimental study on transition of flow pattern and phase distribution in upward air–water two-phase flow along a large vertical pipe," *Int. J. Multiph.*

Flow, vol. 26, no. 3, pp. 367–386, 2000.

[16] S. F. Ali, "Two-phase flow in a large diameter vertical riser," Cranfield University, 2009.

[17] B. J. Azzopardi, S. Taylor, and D. B. Gibbons, "Annular two phase flow in a large diameter tube," Harwell, Oxfordshire, UK, 1982.

[18] G. P. Van der Meulen, "Churn-Annular Gas-Liquid Flows in Large Diameter Vertical Pipes," University of Nottingham, 2012.

[19] N. K. Omebere-Iyari and B. J. Azzopardi, "A Study of Flow Patterns for Gas/Liquid Flow in Small Diameter Tubes," *Chem. Eng. Res. Des.*, vol. 85, no. 2, pp. 180–192, 2007.

[20] P. F. Pickering, G. F. Hewitt, M. J. Watson, and C. P. Hale, "The prediction of flows in production risers - truth and myth?," in *IIR Conference*, 2001, pp. 1–16.

[21] H.-M. Prasser, A. Böttger, and J. Zschau, "A new electrode-mesh tomograph for gas–liquid flows," *Flow Meas. Instrum.*, vol. 9, no. 2, pp. 111–119, 1998.

[22] H.-M. Prasser, D. Scholz, and C. Zippe, "Bubble size measurement using wire-mesh sensors," *Flow Meas. Instrum.*, vol. 12, no. 4, pp. 299–312, 2001.

[23] E. Krepper, D. Lucas, and H. Prasser, "On the modelling of bubbly flow in vertical pipes," vol. 235, no. April 2004, pp. 597–611, 2005.

[24] H.-M. Prasser, M. Beyer, H. Carl, S. Gregor, D. Lucas, H. Pietruske, P. Schütz, and F.-P. Weiss, "Evolution of the structure of a gas–liquid two-phase flow in a large vertical pipe," *Nucl. Eng. Des.*, vol. 237, no. 15–17, pp. 1848–1861, Sep. 2007.

[25] M. J. Da Silva, S. Thiele, L. Abdulkareem, B. J. Azzopardi, and U. Hampel, "High-resolution gas–oil two-phase flow visualization with a capacitance wire-mesh sensor," *Flow Meas. Instrum.*, vol. 21, no. 3, pp. 191–197, Sep. 2010.

[26] R. E. Vieira, M. Parsi, C. F. Torres, B. S. McLaury, S. A. Shirazi, E. Schleicher, and U. Hampel, "Experimental characterization of vertical gas-liquid pipe flow for annular and liquid loading conditions using dual Wire-Mesh Sensor," *Exp. Therm. Fluid Sci.*, vol. 64, pp. 81–93, 2015.

[27] M. Parsi, R. E. Vieira, C. F. Torres, N. R. Kesana, B. S. McLaury, S. A. Shirazi, E. Schleicher, and U. Hampel, "On the effect of liquid viscosity on interfacial structures within churn flow: Experimental study using wire mesh sensor," *Chem. Eng. Sci.*, vol. 130, pp. 221–238, 2015.

[28] A. A. Almabrok, "Gas-Liquid two-phase flow in up and down vertical pipes," Cranfield

University, 2014.

[29] A. M. Aliyu, “Vertical annular gas-liquid two-phase flow in large diameter pipes,” Cranfield University, 2015.

[30] A. M. Aliyu, L. Lao, A. A. Almabrok, and H. Yeung, “Interfacial shear in adiabatic downward gas/liquid co-current annular flow in pipes,” *Exp. Therm. Fluid Sci.*, vol. 72, pp. 75–87, 2016.

[31] Y. Taitel, D. Bornea, and A. E. Dukler, “Modelling flow pattern transitions for steady upward gas-liquid flow in vertical tubes,” *AIChE J.*, vol. 26, no. 3, pp. 345–354, May 1980.

[32] T. Fukano and T. Furukawa, “Prediction of the effects of liquid viscosity on interfacial shear stress and frictional pressure drop in vertical upward gas–liquid annular flow,” *Int. J. Multiph. Flow*, vol. 24, no. 4, pp. 587–603, Jun. 1998.

[33] R. M. MacGillivary and K. S. Gabriel, “A study of annular flow film characteristics in microgravity and hypergravity conditions,” *Acta Astronaut.*, vol. 53, no. 4–10, pp. 289–297, Aug. 2003.

[34] A. Wolf, S. Jayanti, and G. . Hewitt, “Flow development in vertical annular flow,” *Chem. Eng. Sci.*, vol. 56, no. 10, pp. 3221–3235, May 2001.

[35] A. Skopich, E. Pereyra, C. Sarica, and M. Kelkar, “Pipe-diameter effect on liquid loading in vertical gas wells,” *SPE Prod. Oper.*, vol. 30, no. 2, pp. 164–176, 2015.

[36] M. H. S. Zangana, “Film behaviour of vertical gas-Liquid Flow in a large diameter pipe,” University of Nottingham, 2011.

[37] G. F. Hewitt and D. N. Roberts, “Studies of Two Phase Patterns by Simultaneous X-Ray and Flash Photography,” Harwell, Berkshire, 1969.

[38] P. G. Kosky, “Thin liquid films under simultaneous shear and gravity forces,” *Int. J. Heat Mass Transf.*, vol. 14, no. 8, pp. 1220–1224, 1971.

[39] W. H. Henstock and T. J. Hanratty, “The interfacial drag and the height of the wall layer in annular flows,” *AIChE J.*, vol. 22, no. 6, pp. 990–1000, 1976.

[40] J. C. Asali, T. J. Hanratty, and P. Andreussi, “Interfacial Drag and Film Height for Vertical Annular Flow,” *Am. Inst. Chem. Eng.*, vol. 31, no. 6, pp. 895–902, 1985.

[41] W. Ambrosini, P. Andreussi, and B. J. Azzopardi, “A physically based correlation for drop size in annular flow,” *Int. J. Multiph. Flow*, vol. 17, no. 4, pp. 497–507, Jul. 1991.

[42] K. Hori, M. Nakasamomi, K. Nishikawa, and K. Sekoguchi, “On Ripple of Annular Two-

Phase Flow : 3rd Report. Effect of Liquid Viscosity on Characteristics of Wave and Interfacial Friction Factor," *Trans. Japan Soc. Mech. Eng.*, vol. 44, no. 387, pp. 3847–3856, 1978.

[43] C. Berna, A. Escrivá, J. L. Muñoz-Cobo, and L. E. Herranz, "Review of droplet entrainment in annular flow: Interfacial waves and onset of entrainment," *Prog. Nucl. Energy*, vol. 74, pp. 14–43, 2014.

[44] R. M. MacGillivray, "Gravity and Gas Density Effects on Annular Flow Average Film Thickness and Frictional Pressure Drop.," University of Saskatchewan, 2004.

[45] P. Ju, C. S. Brooks, M. Ishii, Y. Liu, and T. Hibiki, "Film thickness of vertical upward co-current adiabatic flow in pipes," *Int. J. Heat Mass Transf.*, vol. 89, pp. 985–995, Oct. 2015.

[46] P. B. Whalley, G. F. Hewitt, and P. Hutchinson, "Experimental Wave and Entrainment Measurements in Vertical Annular Two-phase Flow," Atomic Energy Research Establishment, Harwell, Oxfordshire, UK, 1973.

[47] P. Sawant, M. Ishii, and M. Mori, "Droplet entrainment correlation in vertical upward co-current annular two-phase flow," *Nucl. Eng. Des.*, vol. 238, no. 6, pp. 1342–1352, Jun. 2008.

[48] K. Mishima and M. Ishii, "Flow regime transition criteria for upward two-phase flow in vertical tubes," *Int. J. Heat Mass Transf.*, vol. 27, no. 5, pp. 723–737, May 1984.

[49] L. B. Fore and A. E. Dukler, "Droplet deposition and momentum transfer in annular flow," *AIChE J.*, vol. 41, no. 9, pp. 2040–2046, 1995.

[50] D. Schubring and T. A. Shedd, "Wave behavior in horizontal annular air–water flow," *Int. J. Multiph. Flow*, vol. 34, no. 7, pp. 636–646, 2008.

[51] R. J. Belt, J. M. C. Van't Westende, and L. M. Portela, "Prediction of the interfacial shear-stress in vertical annular flow," *Int. J. Multiph. Flow*, vol. 35, no. 7, pp. 689–697, 2009.

[52] M. B. Alamu, "Simultaneous Investigation of Entrained Liquid Fraction , Liquid Film Thickness and Pressure Drop in Vertical Annular Flow," *J. Energy Resour. Technol.*, vol. 133, pp. 23103-1-23103–10, 2011.

[53] D. F. Tatterson, J. C. Dallman, and T. J. Hanratty, "Drop sizes in annular gas-liquid flows," *AIChE J.*, vol. 23, no. 1, pp. 68–76, Jan. 1977.

[54] D. Schubring and T. A. Shedd, "Critical friction factor modeling of horizontal annular base film thickness," *Int. J. Multiph. Flow*, vol. 35, no. 4, pp. 389–397, 2009.

[55] M. B. Alamu, "Investigation of Periodic Structures in Gas-Liquid Flow," University of

Nottingham, 2010.